

# Multiwavelength cluster mass estimates and machine learning

J.D.Cohn<sup>1,2\*</sup> and Nicholas Battaglia<sup>3</sup>

<sup>1</sup>*Space Sciences Laboratory University of California, Berkeley, CA 94720, USA*

<sup>2</sup>*Theoretical Astrophysics Center, University of California, Berkeley, CA 94720, USA*

<sup>3</sup>*Cornell University, Ithaca, NY 14853, USA*

14 June 2022

## ABSTRACT

One emerging application of machine learning methods is the inference of galaxy cluster masses. Often cluster mass predictions are made from observables by fitting or deriving scaling relations; if multiwavelength measurements are available, these scaling relation based estimates are combined into a likelihood. Here, machine learning is used in a simulation to instead directly combine five multiwavelength measurements to obtain cluster masses. Comparisons of the contributions of each observable to the accuracy of the resulting mass measurement are made using model-agnostic Importance Permutation values, as well as by brute force comparison of different combinations of observables. As machine learning relies upon the accuracy of the training set in capturing the observables, their correlations, and the observational selection function, and the training set originates from simulations, a few ways of testing whether a simulation and observations are consistent are explored as well.

**Key words:**

## 1 INTRODUCTION

Galaxy clusters are the most massive bound structures in the universe and are often complex. This is in part due to their tendencies to be triaxial, to lie in an anisotropic environment at intersections (nodes) of the cosmic web, and to be recently formed. A cluster’s host halo can be characterized by its mass, which characterizes many properties of the gas, galaxies and other quantities within it (for a recent review, see Wechsler & Tinker 2018). Clustering with other halos is also most affected by a cluster’s mass (Kaiser 1984; Cole & Kaiser 1988; Efstathiou et al 1988; Mo & White 1996), although there are secondary (“assembly bias”) effects which are also under study, both for clustering and for other cluster properties, such as number of galaxies within. There also is interest in cluster masses due to the sensitivity of the cluster mass distribution to cosmological parameters (e.g., Voit 2005; Allen, Evrard & Mantz 2011; Borgani & Kravtsov 2011).

A particular cluster boundary definition specifies a cluster’s halo and thus its mass. In a simulation, a definition of where a cluster halo begins and where its environment ends<sup>1</sup> can be precisely applied to find the mass, especially using the

available three dimensional spatial and velocity information. Observationally, it is much harder to disentangle a cluster from its surroundings and from direction dependent effects, and to account for confounding dynamical effects. For example, cluster mass can be traced by the galaxies the cluster hosts (richness), but galaxies are observed in redshift space and thus can lie several Mpc from the cluster but appear to be within it. The hot cluster gas scatters CMB photons en route to us via the Sunyaev-Zel’dovich effect (Sunyaev & Zel’dovich 1972), effectively leaving a shadow on the cosmic microwave background or CMB, but other mass along the line of sight to the cluster can also scatter these photons and thus modify the signal. Weak lensing shear captures all the mass in the cluster, but only as part of capturing all the mass between the galaxy being sheared (located behind the cluster) and us (in front of the cluster). Although X-ray measurements tend to only track the hot gas within the cluster, the dynamical state of the gas can significantly modify estimates, and even for X-ray, projection effects can contaminate the sample (e.g., Ramon-Ceja et al 2019).<sup>2</sup>

Multiwavelength measurements of clusters can be com-

<sup>2</sup> There is also a suggested dynamic cluster ‘edge’ definition based upon velocities and positions of galaxies in a cluster, via their splashback (for example, Adhikari, Dalal & Chamberlain 2014; More, Diemer & Kravtsov 2015) or backsplash (for example, Gill,

\* E-mail: jcohn@berkeley.edu

<sup>1</sup> Given the physics included in the simulation

bined to get a more complete picture of any given individual cluster or of a distribution of clusters. To determine a cluster's mass, often a mass-observable relation is found for each cluster property, e.g. galaxy richness or SZ flux, via a scaling relation. The different mass measurements are then combined in a likelihood to get an improved combined estimate (see Allen, Evrard & Mantz 2011, for a detailed review and discussion). As the scatter between the true and estimated mass for each observable is often due to the cluster's triaxiality, anisotropic environment and other physical cluster properties, the mass estimate errors using different observables can be correlated. The correlations should be represented faithfully in the analysis, or they can impose a bias (see, for example, Allen, Evrard & Mantz 2011; Rykoff et al 2008; Stanek et al. 2010; White, Cohn & Smit 2010; Angulo et al 2012; Shirasaki, Nagai & Lau 2016, for more details and examples of correlations). Correlations are also possible between the scatter in the observable used to select the clusters and observables used to measure the cluster masses.

In this note, machine learning is suggested as a method to obtain multiwavelength mass estimates of a cluster directly from the observational quantities, skipping the intermediate step of matching observations to average relations with mass (scaling relations) and instead going straight to the mass prediction of the combined sample.<sup>3</sup> It follows the philosophy of Ho et al (2019) and earlier papers (Ntampaka et al 2015, 2016, 2017). There, galaxy cluster masses are estimated by using cluster galaxy velocities, but instead of turning all the cluster velocities into a single velocity dispersion and mapping the dispersion into a mass using a mean relation (approximate fit), the individual velocities are given to a machine learning algorithm, to encode the more detailed relations between the different galaxy velocities, their angular positions and the cluster final mass.

Here, using a simulation which has several different multiwavelength mock cluster observations, machine learning is used to (1) calculate the mass directly from the combination of the different multiwavelength observables, without going through a mass estimate for each, (2) compare subsets of multiwavelength measurements to each other to identify which combinations give the smallest scatters and biases in predicting mass, and (3) suggest some tests for whether a given simulation correctly captures correlations between different observables. This latter issue becomes more and more important as reliance upon simulations for analysis increases<sup>4</sup>. Having all multiwavelength mock observations on a single simulation guarantees a shared model for all the observables which are being compared. However, this approach is also limited in its usefulness by the accuracy of the simulation (and how well this accuracy is understood); hence

Knebe & Gibson 2005) radius. It is also used in the caustics Rines et al (2003) method to find cluster masses.

<sup>3</sup> One reason one might expect this approach to be successful is that scatter around the true mass for multiwavelength observations can be analyzed using principal component analysis (Noh & Cohn 2012), where it can be seen that the leading contribution to the scatter for each observable tends to be occur in a certain combination with that of other observables.

<sup>4</sup> This is also important for the usual scaling relations method, if a simulation is used for calibrating the scaling relation.

the interest in identifying additional tests such as discussed below.

Again, using the various observations together in a machine learning algorithm is to be contrasted to mapping each measurement to its average mass relation plus scatter (from a simulation) and then combining probabilities. The hope is that the simultaneous approach might include more information from the relations between the multiwavelength measurements in comparison to mapping to average values for each by some procedure, and then including pairwise correlations in the likelihood. In section §2, the simulation measurements and machine learning methods are described. In section §3.1, mass estimates are made, and errors characterized. In §3.2, a few ways of testing a simulation relative to observations are suggested and explored with a simulation (relative to a simulation with shuffled observables, i.e., with different correlations). §4 concludes.

## 2 METHODS AND DATA

We use a dark matter only simulation in a periodic box of side 200 Mpc  $h^{-1}$  with  $1500^3$  particles, evolved using the TREEPM (White 2002) code, and provided by Martin White. Cluster observables are assigned as in White, Cohn & Smit (2010) (hereafter WCS), which can be consulted for details beyond those found below. The background cosmological parameters are  $h = 0.72$ ,  $n = 0.97$ ,  $\Omega_m = 0.25$ , and  $\sigma_8 = 0.8$ , slightly off from the best estimated current cosmology Planck collaboration (2016), but close enough for the concerns here. There are outputs at 45 times equally spaced in  $\ln(a)$  from  $z = 10$  to 0. Halos are found using a Friends of Friends (FoF) halo finder (Davis et al. 1985), with linking length  $b = 0.168$  times the mean interparticle spacing. Masses quoted below are FoF masses. As the box is fairly small, only  $z = 0.1$  is considered, with 117 halos with  $M > 10^{14} h^{-1} M_\odot$  and 339 halos with  $M > 5 \times 10^{13} h^{-1} M_\odot$ . Mock observations are made of five observables, again, for more details, see WCS.

- $N_{red}$ : red galaxy richness (based on the older MaxBCG mass estimator Koester et al. (2007); colors are assigned using Skibba & Sheth (2009).)
- MF: richness from matched filter based upon Yang, Mo & van den Bosch (2008)
- vel: velocity dispersions
- $Y_{int}$ : Sunyaev-Zel'dovich decrement  $y$  (Sunyaev & Zel'dovich 1972), integrated within a disk of radius  $r_{180b}$
- WL shear: fit to a dispersion  $\sigma_\zeta$  using the  $\zeta$  statistic and a singular isothermal sphere profile

Although the MaxBCG richness is not in standard use anymore, its replacement in several new and upcoming large surveys (**redmapper**, Rykoff et al 2014) does not yet have a halo model or other description which would allow its richness prediction to be reliably calculated for this sample. (There are many other richness estimators possible, see Old et al (2015) for a comparison of several of them, applied to two blinded data sets.) To get more statistics, and to explore the effect of anisotropy, triaxiality, and their correlations, each cluster is "observed" from 96 different isotropically distributed directions on a sphere. The distribution of the resulting observables as a function of mass is shown

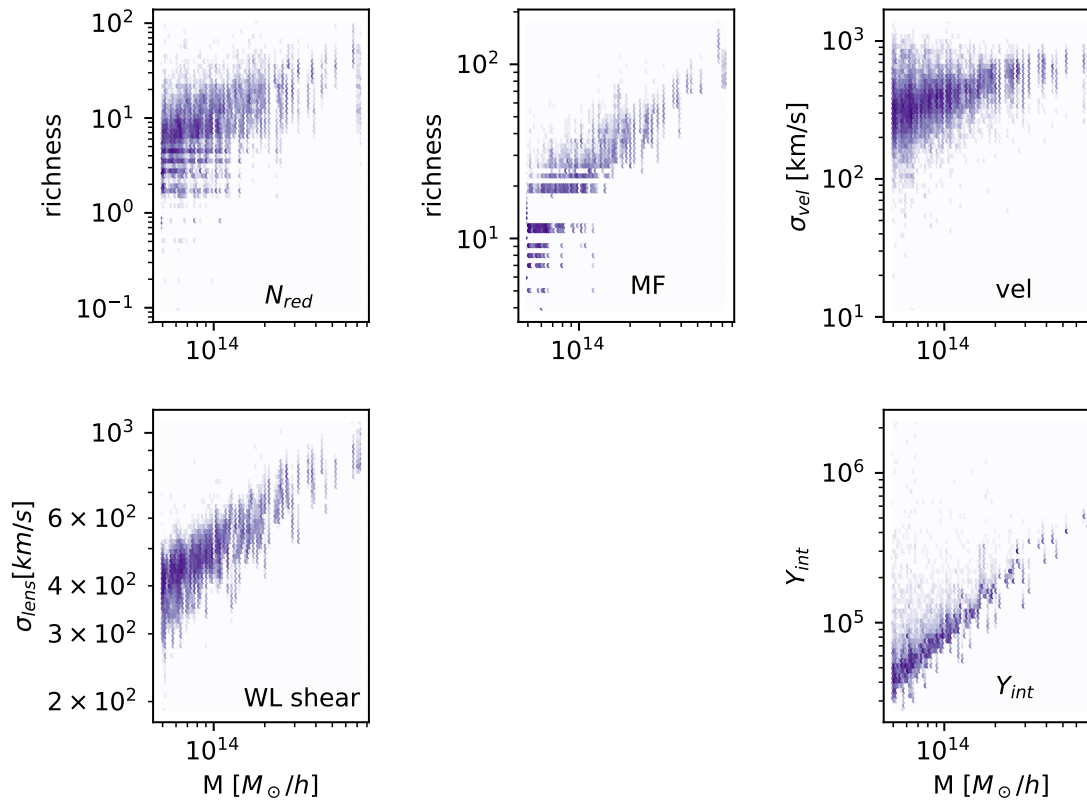


**Figure 1.** Distribution of each observable for all the lines of sight of all halos with  $M > 5 \times 10^{13} h^{-1} M_{\odot}$  in the box.

in Fig. 1. Note that these are meant to be mock observations, that is, to use only information available to an observer (rather than the three dimensional velocities and positions, exact gas content, etc., which a simulator might be able to access.<sup>5</sup>)

For machine learning, these five measurements are the input observables for each cluster; the output is the true mass  $\log_{10} M_{\text{true}}$  for the training set, and the mass prediction  $\log_{10} M_{\text{pred}}$  for the testing set. The training set is a random selection of the set of cluster observations (1/10 of the sample), with testing done on the other 9/10. The machine learning programs used are `GradientBoostingRegressor`, `ExtraTreesRegressor` and `RandomForestRegressor` from `sklearn` in python.<sup>6</sup>

<sup>5</sup> The match between observable and true mass will change and likely decrease somewhat if additional parameters used in the fits are estimated directly from the data. For instance,  $Y_{\text{int}}$  uses the true  $r_{180b}$  as the outer radius for integration.

<sup>6</sup> The exact calls were: `GradientBoostingRegressor(loss='ls', learning_rate=0.1, n_estimators=100, subsample=1.0, criterion='friedman_mse', min_samples_split=2, min_samples_leaf=1, min_weight_fraction_leaf=0.0, max_depth=3, min_impurity_split=None, init=None, random_state=None, max_features=None, alpha=0.9, verbose=0, max_leaf_nodes=None, warm_start=False, presort='auto')` (default values for the arguments, `ExtraTreesRegressor(n_estimators=700, min_samples_split=5, n_jobs=-1)`,

## 3 RESULTS

### 3.1 Predicting mass

The correlation between  $\log_{10} M_{\text{true}}$  and  $\log_{10} M_{\text{pred}}$  for the three machine learning methods are shown in Fig. 2, and lie in the range 95%-96%, listed on the  $y$ -axis for each panel.

To estimate the scatter in true mass for a given predicted cluster mass, the distribution in the simulation must be chosen not according to the unobservable true mass, as in Fig. 2, but according to the same selection function as was used to construct the observed sample. If the simulation can be sampled in the same way as the observations, i.e. with the same cuts on SZ flux  $Y_{\text{int}}$ , etc., and is accurate enough, the true mass distributions can be predicted using the observations and the simulation. One way to estimate the accuracy of  $M_{\text{pred}}$  for an observation, without a particular survey-specific selection function in hand, is to make a cut in  $M_{\text{pred}}$ , based on Fig. 2.<sup>7</sup> This cut can be applied

`RandomForestRegressor(n_estimators=300, n_jobs=-1, min_samples_split=5)`, following Kamdar, Turk & Brunner (2016a,b) for choices of parameters in the function calls.

<sup>7</sup> This cut appears to be complete based upon Fig. 2, and so to the extent the simulation is accurate and thus to be trusted for the machine learning predictions, it can also be used to estimate the regime of applicability. For  $M_{\text{pred}} \geq 10^{14} h^{-1} M_{\odot}$ , it seems all the contributions from the lower mass clusters  $5 \times 10^{13} h^{-1} M_{\odot}$  and above will be captured. Ideally there would be even lower

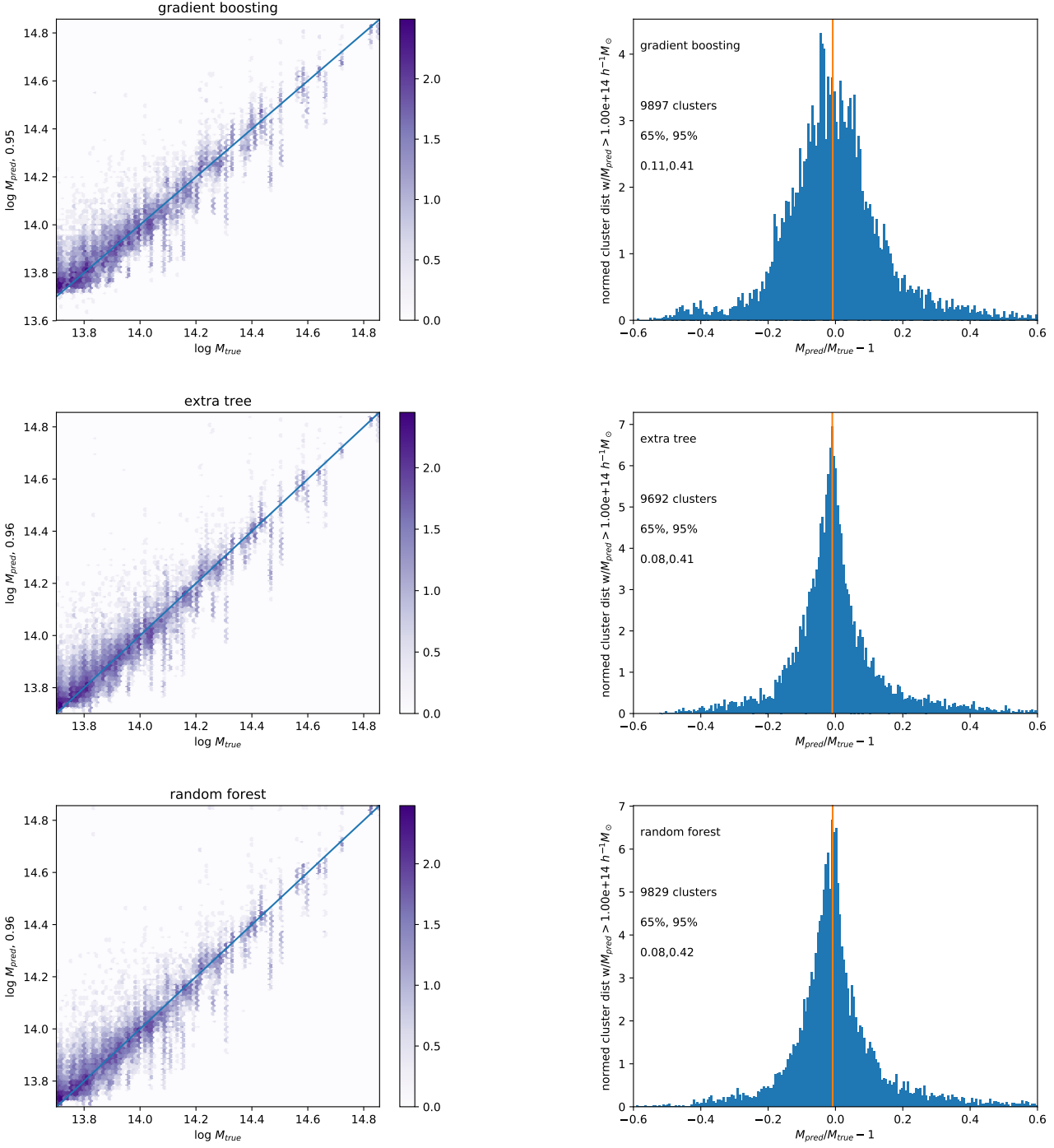


**Figure 2.** True and predicted  $\log_{10} M/(h^{-1}M_{\odot})$  for several different machine learning algorithms, GradientBoost, ExtraTree and RandomForest, top to bottom. The correlation between true and predicted values is shown on the  $y$ -axis. Stripes at fixed  $M_{\text{true}}$  appear because each cluster appears 96 times, observed from 96 different angles. The color scale is  $\log_{10} N_{\text{clusters}}$ .

**Figure 3.** Distribution of  $M_{\text{pred}}/M_{\text{true}} - 1$  for clusters selected with  $M_{\text{pred}} \geq 10^{14} h^{-1} M_{\odot}$ , using GradientBoost, ExtraTree and RandomForest, top to bottom. Clusters are selected with  $M_{\text{pred}} \geq 10^{14} h^{-1} M_{\odot}$  according to each given method (rather than true mass). The 2% of clusters lying in the tails of each distribution are omitted. The values of  $|M_{\text{pred}}/M_{\text{true}} - 1|$  enclosing 65% and 95% of the halos are as listed. The vertical line is the median value, with  $\text{median } M_{\text{pred}}/M_{\text{true}} < 1$ .

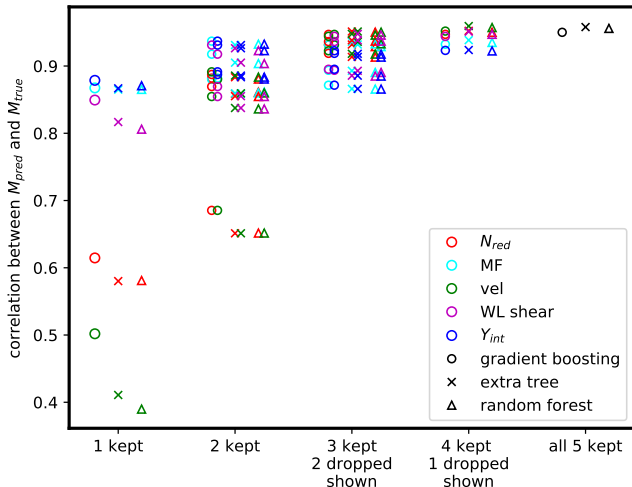


**Figure 4.** Correlations between  $M_{\text{pred}}$  and  $M_{\text{true}}$  when a subset of the observables are used. Colors denote which observables are being used (when one or two are used to calculate  $M_{\text{pred}}$ ) or neglected (when three or four are used to calculate  $M_{\text{pred}}$ ). The three shapes correspond to the three machine learning methods as noted, slightly offset horizontally, for readability. For reference, the results for all measurements, as in Fig. 2, are shown in black at far right.

to both the simulation and observations without knowing the true mass distribution in the observations, and is just a stand-in for a specific but unknown selection function corresponding to a given survey.

For  $M_{\text{pred}} \geq 10^{14} h^{-1} M_{\odot}$ ,  $M_{\text{pred}}/M_{\text{true}} - 1$  is shown in Fig. 3 for the three different ML algorithms also used in Fig. 2. The distributions are not well fit by gaussian or lognormal distributions, so values of  $M_{\text{pred}}/M_{\text{true}} - 1$  encompassing 65% and 95% of the galaxies around the mean are shown. The vertical line is the median  $M_{\text{pred}}/M_{\text{true}}$ , which is slightly less than one.

ExtraTree and RandomForest have narrower scatter in  $M_{\text{pred}}/M_{\text{true}} - 1$  than GradientBoost, and all three histograms have tails to large  $M_{\text{pred}}/M_{\text{true}} - 1$ , comprising the 2% of cluster lines of sight which are not shown. Again, the advantage of this approach is to calculate the mass from the combined measurements all at once. In principle, errors and scaling relations for the usual approach would also have to be calculated from a simulation, using distributions such as are in Fig. 1, with close attention to using the relevant selection function and its correlations with the multiwavelength measurements.<sup>8</sup>

One can also study how well a given subset of the observations predicts mass. Formally one part of this question

mass halos measured with these observations in the simulation, and a larger sample, to confirm lower masses are not being missed with this cut, but these are not available in the current data set.

<sup>8</sup> The effect of these errors on the mass function as a whole was difficult to estimate without adding many other assumptions, as the sample was only large because it was replicated 96 times using different lines of sight.

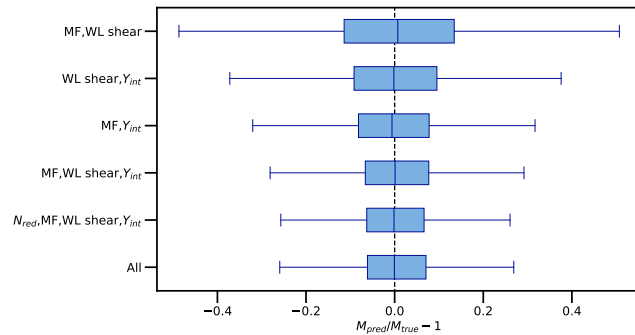


**Figure 5.** The median, 25-75 and 0.35-99.65 percentiles of the  $M_{\text{pred}}/M_{\text{true}} - 1$  distributions (see Fig. 3) for ExtraTree are illustrated with vertical line inside the box, the edges of the box and the whiskers, respectively. The subsets of observables are listed on the y-axis including the entire set of observables (labeled all) at the bottom for reference. From the bottom, the second and third subsets have the vel and  $N_{\text{red}}$  observables cumulatively removed, respectively, as they had lowest Importance Permutation (IP) values. The upper three subsets show permutations of the remaining three observables, MF, WL shear and  $Y_{\text{int}}$ . The  $M_{\text{pred}}/M_{\text{true}} - 1$  distributions upon removing the vel and  $N_{\text{red}}$  observables show little to no change compared to the all the observables, which is consistent with the IP results that they provide the least information. Results are similar for GradientBoost and RandomForest.

is to ask: "how important is each simulated observable when inferring  $M_{\text{pred}}$  (in these simulations)?" In Machine Learning, *Importance Permutation* (IP, e.g. Breiman 2001; Strobl et al. 2008) is a model-agnostic way to determine the relative importance of each observable. In short, the IP procedure uses the difference in the prediction accuracy before and after permuting a given predictor observable to quantify its importance. The IP is generally a reliable except for cases where the observables are highly correlated, which will result in an over-estimation of the highest ranked observables (Strobl et al. 2008). However, the lowest ranking IP will not be biased as the least correlated observables will also have the lowest IP values. Thus, for this particular implementation the IP values are used to determine which observable provide the least information. The lowest ranking observable was vel followed by  $N_{\text{red}}$  for all three machine learning programs, GradientBoost, ExtraTree and RandomForest. The IP values for vel and  $N_{\text{red}}$  ranged from 0.004 to 0.006 and 0.02 to 0.05, respectively, compared to roughly factors of two to ten larger IP values for the other observables. These are the raw IP values, with better statistical properties than the scaled (*z-score*) IP values (e.g., Strobl et al. 2008).

In more (brute force) detail,  $M_{\text{pred}}$  and  $M_{\text{true}}$  correlations are shown in Fig. 4, for all combinations of observables. The circle, cross and triangle symbols denote the three different machine learning methods, and colors the observation or observations included (for using one or two observables) or the observations or observation dropped (when using three or four observables).<sup>9</sup> In correlations, the relative unimpor-

<sup>9</sup> These are based on a cut on true mass. A second step would be again to impose the selection function, but this is very survey dependent, and the simulated sample is very small; the idea

tance of  $N_{\text{red}}$  and  $\text{vel}$  is more visible when  $M_{\text{pred}} - M_{\text{true}}$  is based upon one observable or on these two alone, however, the  $M_{\text{pred}} - M_{\text{true}}$  correlations are also in fact highest when one or the other of these measurements is dropped, rather than  $Y_{\text{int}}$ , WL shear or MF.

The distributions of  $M_{\text{pred}}/M_{\text{true}} - 1$  for the most accurate subsets of mock measurements (in this simulation, with the implicit true mass selection function) can be studied in more detail with "whisker" plots. Fig. 5 illustrates the impact of removing observables on the  $M_{\text{pred}}/M_{\text{true}} - 1$  distributions. Only the ExtraTree distributions are shown in Fig. 5, but the results are similar for the other two machine learning programs. The baseline of all observables is shown for comparison. When the lowest IP observables,  $\text{vel}$  and  $N_{\text{red}}$ , are dropped, the distributions showing little to no change, consistent with their low IP values and the statement that  $\text{vel}$  and  $N_{\text{red}}$  contain the least information for inferring  $M_{\text{pred}}$ . Hence, here the IP values provide an efficient and effective way to reduce the number of observable combinations to consider when exploring the impact of removing observables on the  $M_{\text{pred}}/M_{\text{true}} - 1$  distributions. The upper three whiskers show the distributions corresponding to permutations of pairs of the remaining three observables, MF, WL shear and  $Y_{\text{int}}$ . Of these three, dropping  $Y_{\text{int}}$  causes the most spread in  $M_{\text{pred}}/M_{\text{true}} - 1$ .

### 3.2 Simulation validation

The accuracy of  $M_{\text{pred}}$  depends on the training simulations sufficiently capturing the observables as a function of true mass, the correlations between the observables, and the effects of the selection function. (Other mass estimates using scaling relations and correlations derived from simulations depend upon the accuracy of the simulations as well.<sup>10</sup>)

Simulations and observations can be tested directly for agreement of some properties, such as number counts of clusters with a certain  $Y_{\text{int}}$  or richness, for instance. The accuracy of the relations between simulation observables, used in machine learning or likelihoods, is harder to estimate. (In the likelihood approach to finding masses, this difficulty appears in estimating the accuracy of the simulation in capturing the correlations of mass errors, which include the unmeasured true masses.) All one has in hand are observational quantities. However, if the simulations are sufficiently accurate, it is reasonable to expect that relations between mock observations from the simulation would agree with relations between their counterparts in actual observations.

One possibility is to impose a fixed observational cut on both the simulations and observations, and then measure the correlations of observable quantities in both (e.g., to validate the correlations estimated in Farahi et al 2019). Another possibility is to use the machine learning encoding of joint relations between different observables. If the simulation is sufficiently accurate, the machine learning relations between observables, derived from mock simulation

here is just to give a qualitative sense of how much variation in  $M_{\text{pred}} - M_{\text{true}}$  correlations occurs with (combinations of) different methods.

<sup>10</sup> When the correlations are taken out by marginalization, the form of the relation is required, including the variables upon which it depends, rather than the actual numbers.

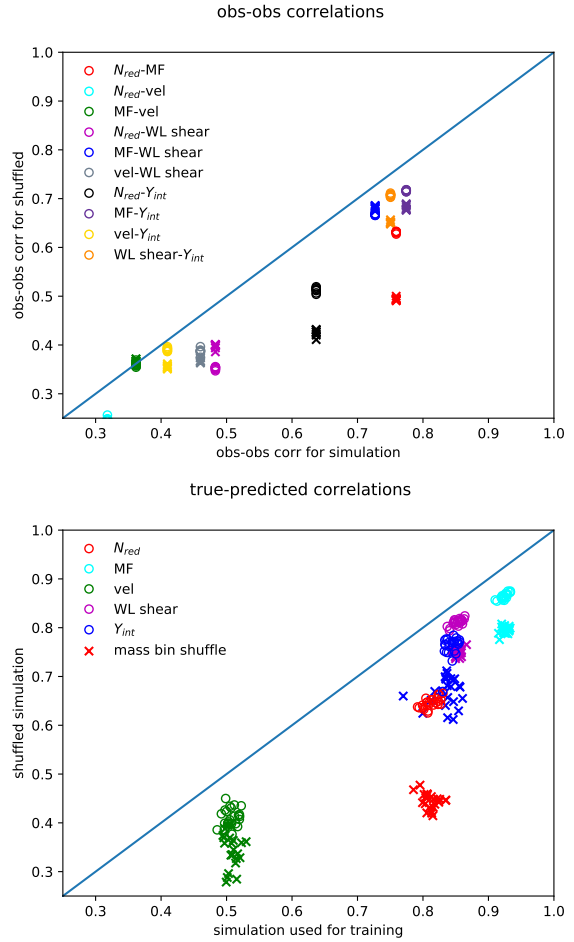


**Figure 6.** Distinguishing between a data set with the same number counts for observables (as in Fig. 1) but different correlations due to shuffling. Two simulations are considered, the original one, and one where cluster properties are shuffled either between clusters within 0.03 dex bins for true mass (crosses) or only between lines of sight for each individual cluster (open circles). Top: correlations between pairs of observables; the correlations for observables for the shuffled clusters are, as expected, lower than the unshuffled ones. Bottom: Correlations between predicted and true values of each of the five observables, separately, when predicted by the other four (x-axis), versus correlations between predictions and true values when the machine learning algorithm trained on the original simulation is tested on each of the two shuffled simulations instead. All 3 machine learning methods are included. The correlation relative to the original simulation degrades more strongly if cluster properties are shuffled within a mass bin, not only between lines of sight. See text for more discussion. Clusters have observed WL shear  $\sigma_{\text{lens}} = 530$  km/s in all cases.

observations, should also hold for actual observations. In particular, machine learning can be used to predict one observable given the others, by training on the observables in the simulation alone (instead of predicting the observationally inaccessible  $M_{\text{pred}}$  as in §3.1). The true and predicted simulation observable pairs, for instance, for  $Y_{\text{int}}$ , can be compared to the true vs. predicted observation observable pairs for  $Y_{\text{int}}$ . Again, crucially, both predictions are based on the simulation training set. If the simulation is close to the observations, the relation of the predictions and true values

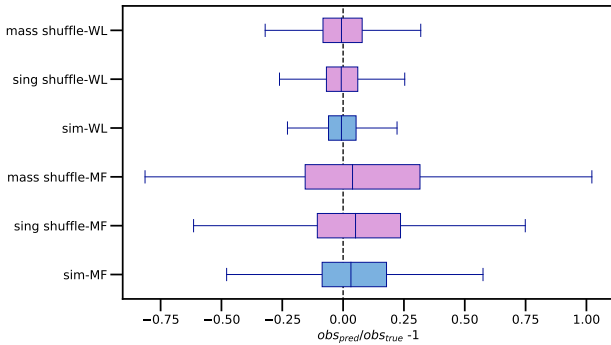


**Figure 7.** Distribution of pred/true WL shear  $\sigma_{\text{lens}} - 1$  (top 3 whiskers) and pred/true MF richness  $-1$  (bottom 3 whiskers) for all clusters in sample, predicted in each case from the other 4 observables. Again, the median, 25-75 and 0.35-99.65 percentiles for ExtraTree are illustrated with vertical central lines, the box edges and the whiskers, respectively. The blue box refers to the training simulation, while the shuffled sightline box (middle of each triplet) and shuffled in 0.03 dex mass bins box (top of each triplet) are in plum. Note that “true” means the value of WL shear  $\sigma_{\text{lens}}$  or MF richness measured in the simulation or observation, respectively. The sample selection function is WL shear  $\sigma_{\text{lens}} > 530 \text{ km/s}$ .

in the mock observations should be similar to the relation of the predictions and true values in the actual observations.

Figures 6 and 7 illustrate these kinds of comparisons between simulations and observations. Given that there is no simulation that agrees with all observations, shuffled variants of the original simulation are taken as “observations”. These shuffled “observations” share number counts but not correlations with the original simulation. Two shufflings are considered: 1) shuffling different lines of sight for each observable, separately for each individual cluster, and 2) shuffling between lines of sight and clusters within 0.03 dex bins in halo mass. This latter not only mixes lines of sight but other effects which might vary between clusters sharing the same mass. Each kind of shuffling is done 8 separate times, to give 16 samples for comparison with the original. To approximate a survey selection function, a cut on WL shear  $\sigma_{\text{lens}}$  of 530 km/s (which seems to reject most low mass halos, see Fig. 1) is made.<sup>11</sup> Shuffling is done after the WL shear cut, to preserve number counts.

In the top panel of Fig. 6, correlations are shown between different simulation observables ( $x$ -axis) and their counterparts for the shuffled variants (“observations,”  $y$ -axis); if the two agreed exactly, the points would lie on the diagonal line. The bottom panel of Fig. 6 compares correlations between machine learning predicted observables and true observables, in the simulation ( $x$ -axis) and in their shuffled counterparts (“observations,”  $y$ -axis). The predicted values of each observable is obtained using the other four via machine learning, trained in both cases on 1/10 of the unshuffled simulation sample. In both, crosses are mass bin

<sup>11</sup> The selection function cuts out many more clusters than the  $M_{\text{pred}}$  selection in §3.1, however, imposing an appropriate  $M_{\text{pred}}$  cut for the shuffled samples seemed to require more steps and assumptions.

shuffled variants, circles are cluster-by-cluster shuffled variants, and colors indicate which observable or observables are involved. Some pair correlations (observable-observable, top panel) or internally predicted quantities (true-pred, bottom panel) change strongly when the original simulation properties are shuffled, but not all.

The simulation and shuffled variants are also compared via whisker plots of machine learning predicted/true  $-1$  values of the fifth observable, for two observables<sup>12</sup> in Fig. 7. Again, the mass shuffled sample is more distinguishable from the original sample than the sample with properties shuffled only cluster by cluster. This may be due to the fact that some of the observable scatter at roughly fixed mass can be attributed to isotropic properties such as the density variations of the local environment<sup>13</sup>.

The above examples show how correlations between observables themselves, correlations between true and machine learning predicted observables and predicted/true ratio distributions could be used to flag disagreements between simulations and observations (in practice, replacing the shuffled simulation in this example with actual sky observations).

## 4 SUMMARY AND DISCUSSION

Three ideas were tried out on a small simulation sample in this note:

- Using machine learning to predict halo masses directly from multiwavelength observations, rather than going through scaling relation mass assignments plus correlated scatter estimates. This produced fairly tight correlations between  $M_{\text{pred}} - M_{\text{true}}$ .
- Comparing the accuracy of machine learning mass predictions for different combinations of multiwavelength measurements, which for this (very small) simulation gave clear answers as to which observable combinations have the most constraining power.
- Testing correlations in simulations (here used to train machine learning) by comparing relations between observables in the simulated mock observations to those in the observations. Testing is done by correlating observables within the simulated or observational data sets directly or via machine learning, in the latter case using one training sample to make predictions for both the simulations and the observations. For the example here, observations with different correlations were generated from the simulation by shuffling the different multiwavelength measurements between lines of sight, either for each cluster separately, or in mass bins. Differences were seen between the simulation and its shuffled counterparts for almost all variations of these tests.

A more extensive simulated data set would allow all of

<sup>12</sup> `ExtraTreeRegressor` was used here as it gave the highest correlations between true and predicted for the original simulation.

<sup>13</sup> We thank M. White for emphasizing this point.

these ideas to be both better tested and better applied<sup>14</sup> and could have:

- larger volume and thus more clusters (there are larger simulations in the literature with with several different observables, e.g., Angulo et al 2012). A larger sample might also allow using fewer lines of sight per cluster, to test for and if need be get rid of possible effects introduced by related lines of sight in the small sample used here. In particular, there were only a small number of different masses at the high mass end, making it difficult to estimate the effect of the machine learning mass errors on the mass function.<sup>15</sup>
- more simulated rather than “painted on” physical properties, for instance, using hydrodynamics to capture more of the baryonic effects during evolution (e.g., Shirasaki, Nagai & Lau 2016; Henson et al 2017), and more generally, improvements of mock observations.
- more cluster observables (X-ray, for instance, or other richness estimators<sup>16</sup>); the velocity information used in Ntampaka et al (2015, 2016, 2017); Ho et al (2019) could certainly be added.
- more simulated observations of smaller mass halos and other possible configurations which might also pass the cluster selection cuts (depending upon the cluster finding algorithm, i.e., sample selection).

For mass predictions, improved machine learning algorithms are likely possible. In addition, it would be good to know if there are better ways than simply sampling, as is done here, to estimate the error on  $P(M_{\text{true}}|M_{\text{pred}})$  as found by these machine learning approaches (such as using a “prediction interval”). For the whole sample, the distribution of predictions from a simulation is a good first estimate of these probabilities, assuming the simulation is a representative sampling, but it would be very good to have a way to analyze smaller distributions of observed clusters, down to, for example, using extensive multiwavelength measurements of a single cluster to estimate the likelihood that the cluster came from the same distribution as that of a given simulation. The scatter in  $P(M_{\text{true}}|M_{\text{pred}})$  in Fig. 3 seems fairly small, but in practice would have to be calculated with a better simulation as described above, and the errors above would need to be combined with the uncertainties going into the simulation (see, for example, estimates in Shirasaki, Nagai & Lau (2016) for an enumeration of some of these).

In testing the simulations for accuracy, perhaps further information (such as “importance”) could be used to inform the simulation if the observations and simulations, do

<sup>14</sup> For a more refined comparison of correlations, for example, one could consider smaller bins in some observable, for instance, clusters which lie in a specific WL shear bin, more similar to Farahi et al (2019), rather than just above a minimum value as done here in §3.2.

<sup>15</sup> The small number of true masses in this sample may have also had some effect on the success of ML. For DecisionTreeRegressor, for instance, the success rate is extremely high. The small number of true masses doesn’t seem to be an issue in the other machine learning methods, but would be good to have a larger sample to better sample the space of possible clusters.

<sup>16</sup> Many of the galaxy based cluster mass estimators have been compared in Old et al (2015).

not match sufficiently, and more sophisticated definitions of “match” could be used. It would also be good to incorporate the observational measurement error bars into the simulation tests, perhaps by using a distribution of observational input measurement values weighted by their likelihood. As the errors are different in observations and in the simulations, it seems that training on observations might also be possible (to predict one observable from the others), but one of the two training sets is likely preferable. In addition, the shuffling test here is similar to the analysis made setting the correlations to zero in Shirasaki, Nagai & Lau (2016); that is, the two sorts of correlations are the ones in the simulation and their decorrelated counterpart. It is not clear how a different correlation (rather than a decorrelating shuffling) would appear in these tests.

To summarize, matching each observable to a mass and then combining mass predictions relies upon calibrating each mass prediction separately, while combining the observables first, as suggested here, relies upon a joint calibration from a simulation capturing all observed properties. This machine learning based approach requires a more detailed simulation, but as some of the underlying physics is shared between observables, this approach may have the benefit of including more of the true correlations.<sup>17</sup> Both approaches are incorporating physical assumptions about clusters and their masses, but in different ways.

We thank M. White for the simulations and discussions and G. Evrard for suggestions on an early draft. The simulations used in this paper were performed at the National Energy Research Scientific Computing Center and the Laboratory Research Computing project at Lawrence Berkeley National Laboratory.

## REFERENCES

- Adhikari, S., Dalal, N., Chamberlain, R.T., 2014, JCAP, 11, 19
- Allen, S.W., Evrard, A.E., Mantz, A.B., 2011, ARA&A, 49, 409
- Angulo, R. E., Springel, V., White, S. D. M., Jenkins, A., Baugh, C. M., Frenk, C. S., 2012, MNRAS, 426, 2046
- Borgani S., Kravtsov A., 2011, Adv. Sci. Lett., 4, 204
- Breiman L., 2001, Machine Learning, 45, 5
- Cole, S., Kaiser, N., 1988, MNRAS, 233, 637
- Davis M., Efstathiou G., Frenk C.S., White S.D.M., 1985, ApJ, 292, 371
- Efstathiou G., Frenk C. S., White S. D. M., Davis M., 1988, MNRAS, 235, 715
- Farahi, A., et al, 2019, arxiv:1903.08042
- Gill, S.P.D., Knebe, A., Gibson, B.K., 2005, MNRAS, 356, 1327
- Henson, M. A., Barnes, D. J., Kay, S. T., McCarthy, I. G., Schaye, J., 2017, MNRAS, 465, 3361
- Ho, M., Rau, M.M., Ntampaka, M., Farahi, A., Trac, H., Poczos, B., 2018, arxiv:1902.05950
- Kaiser N., 1984, ApJL, 284, L9

<sup>17</sup> Another possibility is to go even further with machine learning, to cosmological parameters, skipping the calculation of cluster masses along the way. We thank G. Holder for this suggestion.



- Kamdar, H.M., Turk, M.J., Brunner, R.J., 2016a, MNRAS, 455, 642
- Kamdar, H.M., Turk, M.J., Brunner, R.J., 2016b, MNRAS, 457, 1162
- Koester B.P., et al., 2007, ApJ, 660, 221
- Mo H. J., White S. D. M., 1996, MNRAS, 282, 347
- More,S., Diemer, B., Kravtsov, A.V., 2015, ApJ, 810, 36
- Noh, Y., Cohn, J.D., 2012, MNRAS, 426, 1829
- Ntampaka, M., Trac, H., Sutherland, D. J., Battaglia, N., Pczos, B., Schneider, J., 2015, ApJ, 803, 50
- Ntampaka, M., Trac, H., Sutherland, D. J., Fromenteau, S., Pczos, B., Schneider, J., 2015, ApJ, 831, 135
- Ntampaka, M., Trac, H., Cisewski, J., Price, L. C., 2017, ApJ, 835, 106
- Old, L., et al, 2015, MNRAS, 449, 1897
- Planck collaboration: Ade et al, 2016, A & A, 594A, 13
- Ramos-Ceja, M.E.,Pacaud, F., Reiprich, T.H., Migkas, K., Lovisari, L., Schellenberger, G., 2019, arXiv:1904.10275
- Rines, K., Geller, M.J., Kurtz, J.J., Diaferio, A., 2003, AJ, 126, 2152
- Rykoff, E.S., et al., 2008, MNRAS Letters, 387, 28
- Rykoff, E.S., et al, 2014, ApJ, 785, 104
- Shirasaki, M., Nagai, D., Lau, E.T., 2016, MNRAS, 460, 3913
- Skibba R.A., Sheth R.K., 2009, MNRAS, 392, 1080
- Stanek, R., Rasia, E., Evrard, A.E., Pearce, F., Gazzola, L., 2010, MNRAS, 403, 1072
- Strobl C., Boulesteix A-L., Zeileis A., Hothorn T., 2007 BMC Bioinformatics, 8, 25
- Strobl C., Boulesteix A-L., Kneib T., Augustin T., Zeileis A., 2008, BMC Bioinformatics, 9, 307
- Sunyaev R.A., Zel'dovich Ya.B., 1972, Comments on Astrophysics and Space Physics, 4, 173
- Voit G. M., 2005, Reviews of Modern Physics, 77, 207
- Wechsler, R.H., Tinker, J.L., 2018, ARA&A, 56, 435
- White M., 2002, ApJS, 143, 241
- White, M., Cohn, J.D., Smit, R., 2010, MNRAS, 408, 1818
- Yang X., Mo H.J., van den Bosch F.C., 2008, ApJ, 676, 248